Available online at www.sciencedirect.com
SCIENCE DIRECT®
Journal of Theoretical Biology 222 (2003) 307–322
Journal of Theoretical Biology
www.elsevier.com/locate/jtbi

The dynamics of single-substrate continuous cultures: the role of transport enzymes

Jason Shoemaker[a], Gregory T. Reeves[b], Shakti Gupta[a], Sergei S. Pilyugin[c], Thomas Egli[d], Atul Narang[a,*]

[a] Department of Chemical Engineering, University of Florida, Gainesville, FL 32611-6005, USA
[b] Department of Chemical Engineering, Princeton University, Princeton, NJ 08544, USA
[c] Department of Mathematics, University of Florida, Gainesville, FL 32611-8105, USA
[d] Department of Microbiology, EAWAG, CH-8600, Dübendorf, Switzerland

Received 9 July 2002; received in revised form 17 November 2002; accepted 9 December 2002

Abstract

A chemostat limited by a single growth-limiting substrate displays a rich spectrum of dynamics. Depending on the flow rate and feed concentration, the chemostat settles into a steady state or executes sustained oscillations. The transients in response to abrupt increases in the flow rate or the feed concentration are also quite complex. For example, if the increase in the flow rate is small, there is no perceptible change in the substrate concentration. If the increase in the flow rate is large, there is a large increase in the substrate concentration lasting several hours or days before the culture adjusts to a new steady state. In the latter case, the substrate concentration and cell density frequently undergo damped oscillations during their approach to the steady state. In this work, we formulate a simple structured model containing the inducible transport enzyme as the key intracellular variable. The model displays the foregoing dynamics under conditions similar to those employed in the experiments. The model suggests that long recovery times (on the order of several hours to several days) can occur because the initial transport enzyme level is too small to cope with the increased substrate supply. The substrate concentration, therefore, increases until the enzyme level is built up to a sufficiently high level by the slow process of enzyme induction. Damped and sustained oscillations can occur because transport enzyme synthesis is autocatalytic, and hence, destabilizing. At low dilution rates, the response of stabilizing processes, such as enzyme dilution and substrate consumption, becomes very slow, leading to damped and sustained oscillations.

Keywords: Microbial growth; Chemostat; Mathematical model; Transients; Steady states; Oscillations

1. Introduction

Among the most pressing problems in bioengineering is the dynamic response of a chemostat. To the practicing engineer, the steady state represents a theoretical construct rarely realized in practice. Indeed, industrial bioreactors are inevitably insulted with flow rate and feed concentration fluctuations. These unavoidable perturbations often result in large overshoots of the substrate concentrations, causing regulatory violations in wastewater treatment plants and product deterioration in industrial fermenters. A mathematical theory of chemostat dynamics is of utmost importance for developing rational operating protocols and optimal control strategies.

Models of microbial growth have been classified into two categories. Experiments show that overshoots of substrate concentration occur when cells in a starved state are suddenly exposed to large substrate concentrations by increasing the feed flow rate or concentration. Two factors could contribute to this phenomenon.

1. Either the starved cells lack the enzyme that transports the substrate from the medium into the cell, and a considerable length of time is required to synthesize the enzyme to a level that is high enough to match the increased supply of substrate.
2. Or the starved cells lack the ribosomal machinery required to convert the catabolic products derived from the substrate into biomass, and the resultant

*Corresponding author. Tel.: +1-352-392-0028; fax: +1-352-392-9513.
E-mail address: narang@che.ufl.edu (A. Narang).

0022-5193/03/$ - see front matter © 2003 Elsevier Science Ltd. All rights reserved.
doi:10.1016/S0022-5193(03)00036-5

accumulation of the catabolic products represses substrate uptake by inhibiting the transport enzyme. This repression persists until the ribosomal machinery has been built to a level consistent with the increased supply of substrate (Maaloe and Kjeldgaard, 1966).

Given the important role of these intracellular variables, it is clear that *unstructured* models cannot provide a satisfactory explanation of this phenomenon. These models assume that the specific growth rate of the cells is completely determined by the substrate concentration, and hence, it adjusts instantaneously to changes in the substrate concentration (Tsuchiya et al., 1966). The data, on the other hand, shows that when the chemostat is subjected to large perturbations, only part of the adjustment occurs instantaneously. Part of it occurs slowly because enzymes or/and ribosomes must be synthesized to fully adjust to the new conditions (Mateles et al., 1965). *Structured* models take due account of the fact that the specific growth rate depends on the substrate concentration and appropriate intracellular variables, namely, enzymes or/and ribosomes.

Several structured models have been proposed in order to capture single-substrate dynamics. These include highly structured models accounting for maintenance, storage, and synthesis of ribosomes and various enzymes (Baloo and Ramkrishna, 1990; Domach et al., 1984). The goal of this work is to study the global dynamics of single-substrate growth by considering a simple structured model. We assume, in particular, that there is no maintenance, and that "excess" ribosomes are always available, so that the sluggish response of a chemostat, whenever it occurs, is exclusively due to low transport enzyme levels in the cells. This is not to deny the roles of maintenance and ribosomal synthesis, but to determine the extent to which enzyme synthesis alone can account for the observed lags. Experiments show that in *Escherichia coli*, the assumption of "excess" ribosomes is valid for dilution rates up to 0.4 1/h.

1. If the dilution rate is shifted up from 0.4 1/h to 0.8 1/h, the specific growth rate increases almost instantaneously to 0.6 1/h (Mateles et al., 1965). This implies that de novo synthesis of ribosomes is not required to improve upon the prevailing specific growth rate of 0.4 1/h. Similar results have been obtained by others (Harvey, 1970; Koch and Deppe, 1971).
2. The concentration of ribosomal RNA, the key constituent of ribosomes, is constant for dilution rates up to 0.4 1/h. Within this range of dilution rates, the protein synthesis rate is improved by increasing not the level of ribosomes, but the speed with which ribosomes move along the messenger RNA during protein synthesis (Neidhardt et al., 1990, p. 421).

An approach similar to ours was followed in previous studies. Powell assumed that the specific growth rate was proportional to the concentration of an unindentified intracellular entity called "Q-substance" which was synthesized autocatalytically at a rate proportional to its concentration (Powell, 1969); this model is formally similar to our model if the "Q-substance" is identified as the transport enzyme. Powell showed that his simulations were in good agreement with the dilution rate shift-up data in ammonia-limited cultures obtained by Mateles et al. (1965). In a more stringent test of the model, Chi and Howell (1976) compared the predictions of Powell's model with dilution rate and feed concentration shift-up data in phenol-limited cultures (Chi and Howell, 1976). Here again, the model predictions were in good agreement with the data, except at large feed concentrations when substrate inhibition became very pronounced. In this work, we extend these studies in two directions. First, we consider a model that takes due account of the mechanism of enzyme synthesis. Specifically, we replace the hyperbolic enzyme synthesis kinetics assumed in our earlier study (Narang, 1998) by sigmoidal kinetics. The sigmoidal kinetics obtain from a careful consideration of the mechanism for enzyme induction (Chung and Stephanopoulos, 1996; Yagil and Yagil, 1971). As we show later, the assumption of sigmoidal kinetics has a profound effect on the dynamics. Second, we do a complete nonlinear analysis of the model which allows us to establish a correspondence between the experimental observations and the relevant notions of dynamical systems theory. We show, in particular, that the long lags occur because the orbits reach the vicinity of a saddle point; damped and sustained oscillations occur because a Hopf bifurcation occurs at low dilution rates. By appealing to this analysis, we are able to give simple physical explanations of these dynamics.

We begin in Section 2 by recapitulating the main features of the model. Single-substrate cultures are generally subjected to one or more of the following three perturbations

1. Dilution rate shifts wherein the dilution rate is shifted at a fixed feed concentration.
2. Feed concentration shifts wherein the feed concentration is shifted (without altering the identity of the substrate).
3. Feed switches wherein the identity of the substrate in the feed is altered.

In Section 3, we simulate the dynamics corresponding to each of these perturbations, and compare our results to the experimental data. Finally, the key conclusions are summarized in Section 4.

2. Model

The kinetic scheme is shown in Fig. 1. Here, S denotes the substrate, E denotes the inducible enzyme or "lumped" system of inducible enzymes catalysing the uptake and peripheral catabolism of S, X denotes the inducer for E, P denotes the "lumped" pool of biosynthetic precursors, and C^- denotes all constituents of cell mass except E, X, and P. The entire cell consisting of E, X, P and C^- is denoted by C. The concentrations of these entities are denoted by the corresponding lower-case letters s, c, e, x, p, and c^-. Here, s (g/l) and c (gdw/l) are based on the volume of the chemostat, whereas x, e, p and c^-(g/gdw) are based on the dry weight of the biomass. Steady state and quasi-steady state concentrations are denoted by overlaying these letters with $\sim$ and $-$, respectively (for instance, $\tilde{x}$ and $\bar{x}$). The yield, denoted Y, is the mass of P produced per unit mass of X.

The following assumptions are made about the kinetics of the various processes

1. The specific substrate uptake rate, denoted r_s, satisfies the kinetic law

$$r_s \equiv V_s e \frac{s}{K_s + s}.$$

2. The specific rate of breakdown of X into energy and precursors P, denoted r_x, is given by

$$r_x \equiv k_x x.$$

3. The specific rate of formation of C^- is given by

$$r_p \equiv k_g p.$$

4. The specific rate of enzyme synthesis, denoted r_e, is

$$r_e \equiv V_e \frac{1 + K_1 x + K_2 x^2}{K_3 + K_1 x + K_2 x^2}.$$

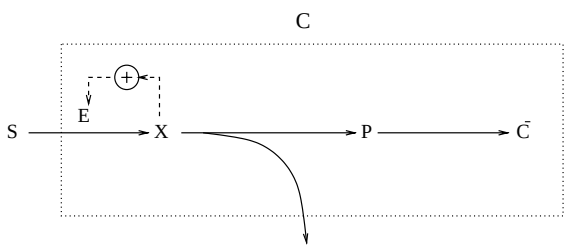

Fig. 1. Kinetic scheme of the model. Here, S denotes the substrate, X denotes the inducer, E denotes the inducible enzyme(s) catalysing the uptake and peripheral catabolism of S, P denotes the biosynthetic precursors derived from catabolism of X, C^- denotes the remaining components of biomass, and C denotes the entire cell consisting of E, X, P and C^-. The positive feedback loop represents the induction of enzyme synthesis.

These kinetics obtain because the repressor can bind to two inducer molecules (Yagil and Yagil, 1971). Thus, K_1 is the equilibrium constant for binding of a repressor to one inducer molecule, K_2 is the equilibrium constant for binding of a repressor to two inducer molecules, and K_3 is proportional to the equilibrium constant for binding of a repressor to an operator.

In what follows, we shall appeal to the following two facts. First, since repressor-operator binding is not perfectly tight, i.e. K_3 is finite, the enzyme is synthesized even in the absence of the inducer; this phenomenon is referred to as *constitutive* enzyme synthesis. Second, if $K_2 \gg K_1^2$, as is the case for the *lac* operon, binding of the first inducer molecule to a repressor facilitates the binding of the second inducer molecule, resulting in cooperative or sigmoidal kinetics.

5. The specific rate of enzyme degradation, denoted r_d, follows first-order kinetics

$$r_d \equiv k_d e.$$

6. The yield, Y, is a fixed "stoichiometric" coefficient. That is, the rates of non-biosynthetic processes, such as overflow metabolism, energy spillage, and maintenance, are proportional to the biosynthetic rate.

A mass balance on the state variables yields

$$\frac{ds}{dt} = D(s_f - s) - r_s c, \tag{1}$$

$$\frac{dx}{dt} = r_s - r_x - \left(D + \frac{1}{c}\frac{dc}{dt}\right)x, \tag{2}$$

$$\frac{dp}{dt} = Y r_x - r_e + r_d - r_p - \left(D + \frac{1}{c}\frac{dc}{dt}\right)p, \tag{3}$$

$$\frac{de}{dt} = r_e - r_d - \left(D + \frac{1}{c}\frac{dc}{dt}\right)e, \tag{4}$$

$$\frac{dc^-}{dt} = r_p - \left(D + \frac{1}{c}\frac{dc}{dt}\right)c^-, \tag{5}$$

where the last term in Eqs. (2)–(5) represents the dilution of X, P, E, and C^-, respectively, by effluent flow and growth, s_f denotes the concentration of S in the feed, and D denotes the dilution rate. It is shown in (Narang, 1998) that since

1. The mass fraction of all intracellular entities equals unity

$$x + p + e + c^- = 1 \text{ g/gdw}.$$

2. The inducer and precursor concentrations rapidly achieve quasi-steady state

$$\frac{dx}{dt} = \frac{dp}{dt} = 0 \quad \Rightarrow \quad r_x \approx r_s, \quad r_p \approx Y r_x$$

Eqs. (1)–(5) are approximated by the equations

$$\frac{ds}{dt} = D(s_f - s) - \left(V_s e \frac{s}{K_s + s}\right)c, \tag{6}$$

$$\frac{de}{dt} = V_e \frac{1 + K_1\bar{x} + K_2\bar{x}^2}{K_3 + K_1\bar{x} + K_2\bar{x}^2} - \left(YV_s e \frac{s}{K_s + s} + k_d\right)e, \tag{7}$$

$$\frac{dc}{dt} = \left(YV_s e \frac{s}{K_s + s} - D\right)c, \tag{8}$$

$$k_x\bar{x} = V_s e \frac{s}{K_s + s}, \tag{9}$$

$$k_g\bar{p} = YV_s e \frac{s}{K_s + s} \tag{10}$$

for all but a negligibly small initial time interval.

3. Simulations and analysis

The simulations were done with the parameter values for the *lac* operon (Table 1). Appendix A contains the basis for order-of-magnitude estimates of these parameters. Appendix B contains a detailed comparison of the model simulations and experimental observations for various types of perturbations.

3.1. Steady states

Eqs. (6)–(10) admit two types of steady states, namely, the persistence ($\tilde{c} \neq 0$) and the washout ($\tilde{c} = 0$) steady states; we denote them by ϕ_1 and ϕ_0, respectively.

The persistence steady state, ϕ_1, is unique, no matter what the parameter values. At the persistence steady state, the specific growth rate equals the dilution rate; that is

$$YV_s\tilde{e}\frac{\tilde{s}}{K_s + \tilde{s}} = D. \tag{11}$$

It immediately follows that

$$\tilde{x}(D) = \frac{D}{Yk_x}, \tag{12}$$

$$\tilde{p}(D) = \frac{D}{k_g}, \tag{13}$$

$$\tilde{e}(D) = \frac{1}{D + k_d}\left[V_e \frac{1 + K_1\tilde{x} + K_2\tilde{x}^2}{K_3 + K_1\tilde{x} + K_2\tilde{x}^2}\right], \tag{14}$$

Table 1
Parameter values used in the simulations

$V_s = 10^4$ g/g-h	$K_s = 10^{-2}$ g/l	$Y = 0.4$ g/g
$k_x = 900$ g/g-h	$V_e = 2 \times 10^{-4}$ g/gdw-h	$K_1 = 10^5$ gdw/g
$K_2 = 10^{11}$(gdw/g)^2	$K_3 = 10^5$	$k_d = 10^{-2}$ 1/h

$$\tilde{s}(D) = K_s \frac{D}{YV_s\tilde{e} - D}, \tag{15}$$

$$\tilde{c}(D, s_f) = Y(s_f - \tilde{s}). \tag{16}$$

On the other hand, depending on the parameter values, there can be up to three washout steady states. To see this, observe that $\tilde{s} = s_f$ at a washout steady state. It follows from Eq. (15) that washout dilution rates satisfy the equation

$$\tilde{s}(D) = K_s \frac{D}{YV_s\tilde{e}(D) - D} = s_f. \tag{17}$$

This equation typically admits one or three positive solutions. For, if K_2 is large, then $\tilde{s}(D)$ has two local extrema (Fig. 2). Intuition suggests that $\tilde{s}(D)$ should be a monotonically increasing function of D. That $\tilde{s}(D)$ *decreases* with respect to D over a certain range of dilution rates can be attributed to the fact that at large K_2, the kinetics of enzyme induction are sigmoidal. Thus, there is a range of dilution rates over which $\tilde{e}(D)$ increases as the square of the dilution rate (see Fig. 3). It follows that from Eq. (11) that if $\tilde{e}(D)$ increases faster than D, then $\tilde{s}(D)$ must necessarily decrease. The non-monotonicity of $\tilde{s}(D)$ implies that there exist two positive values $s_f^- < s_f^+$ such that any intermediate value $s_f^- < s_f < s_f^+$ provides three solutions $D_w^1 < D_w^2 < D_w^3$ of Eq. (17). On the contrary, if s_f is small ($s_f < s_f^-$) or if s_f is large ($s_f > s_f^+$) then Eq. (17) admits a unique washout dilution rate D_w. If K_2 is small, the kinetics of enzyme synthesis are hyperbolic, so that $\tilde{e}(D)$ cannot increase faster than D. Hence, $\tilde{s}(D)$ increases monotonically, and any value of s_f gives a unique washout dilution rate D_w. For the parameter values in Table 1, $\tilde{s}(D)$ has the form shown in Fig. 2 with $s_f^- \simeq 0.002$ g/l and $s_f^+ \simeq 0.02$ g/l. If $s_f = 1.5$ g/l, there is a unique washout dilution rate at $D_w \simeq 0.8$ 1/h; if $s_f = 0.01$ g/l, there are three washout dilution rates at $D_w^1 \simeq 0.0005$ 1/h, $D_w^2 = 0.004$ 1/h, and $D_w^3 = 0.50$ 1/h.

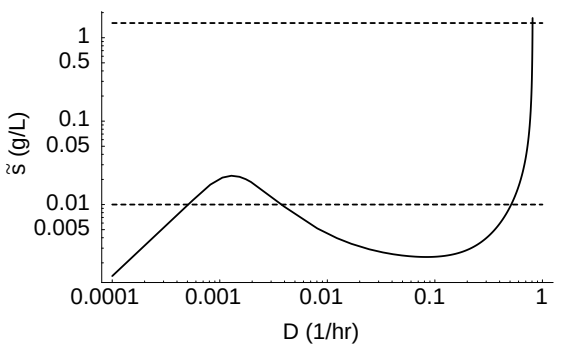

Fig. 2. The existence of multiple critical dilution rates at large K_2. Since the steady-state substrate concentration, $\tilde{s}$, is a non–monotonic function of the dilution rate, there can be three critical dilution rates for $0.002\ \text{g/l} < s_f < 0.02\ \text{g/l}$.

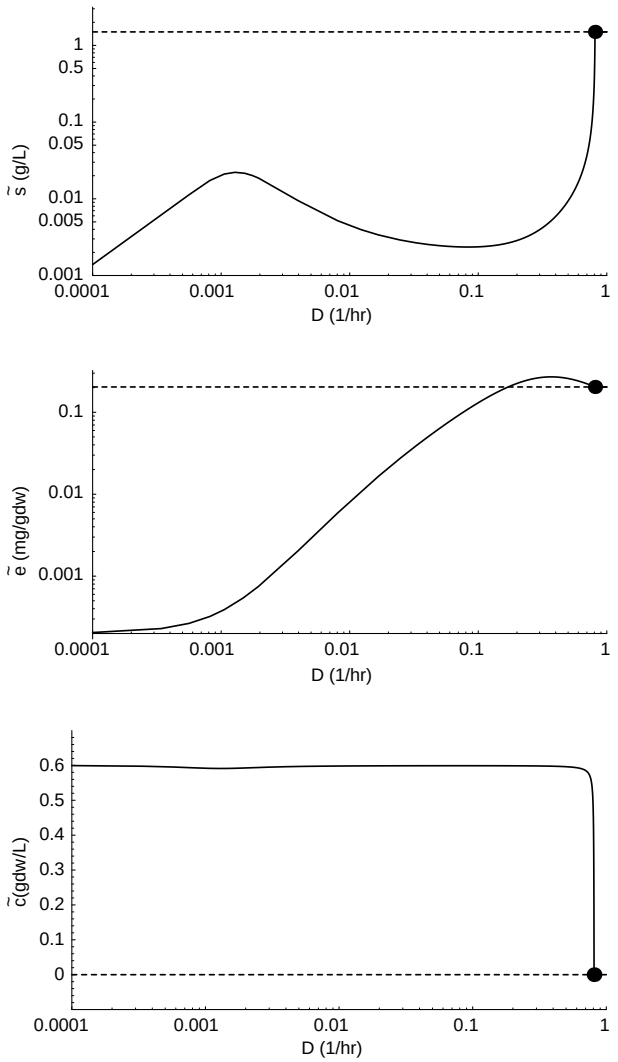

Fig. 3. Variation of steady states with D at $s_f = 1.5$ g/l. The washout bifurcation point is denoted by the symbol •. Stable and unstable steady states are denoted by full and dashed lines, respectively.

3.2. High feed concentrations

In this section, we summarize the experimental data and simulate the model transients at large feed concentrations ($s_f = 1.5$ g/l). Under these conditions, there is a unique washout dilution rate at $D_w = 0.8$ 1/h, and the bifurcation diagram is formally similar to the bifurcation diagram for the Monod model (Fig. 3). Below the (unique) washout dilution rate, the persistence steady state is globally stable; above the washout dilution rate, the washout steady state is globally stable. At low feed concentrations, the bifurcation diagram and dynamics of the model can be more complex; we defer this discussion to Section 3.3.

3.2.1. Dilution rate shifts

In these experiments, at $t<0$, the culture is in a steady state at some dilution rate, say D_0, and feed concentration, s_f. At $t = 0$, the dilution rate is shifted up to a new value, $D > D_0$, while the feed concentration, s_f, is held fixed. In response to this perturbation, it is observed that (Mateles et al., 1965)

1. Almost instantaneously, the substrate concentration and specific growth rate increase, and the cell density decreases.
2. If the shift-up, $D - D_0$, is small, the higher specific growth rate thus achieved equals the higher dilution rate, D. In this case, the change in the substrate concentration and cell density is imperceptibly small.
3. If the shift-up, $D - D_0$, is large, the higher specific growth rate achieved on the fast time-scale falls short of the dilution rate, D. The rapid increase of the specific growth rate is followed by a period of slow increase during which s increases and c decreases. After several hours or days (see, for instance, Standing et al. (1972)), the specific growth rate of the culture catches up with the increased dilution rate. At this instant, s reaches a maximum and c attains a minimum. Thereafter, the specific growth rate is higher than D; during this period, s decreases and c increases until the culture reaches a new steady state consistent with the new dilution rate D.

We show below that all three features are mirrored by the model.

It turns out that the dynamics in response to a dilution rate shift are determined by a two-dimensional system. To see this, it is convenient to replace the cell density, c, by the *potential* cell density, $c_p \equiv c + Ys$; this may be viewed as the cell density that would be realized if the residual substrate were also converted to biomass. One then arrives at the equations

$$\frac{ds}{dt} = D(s_f - s) - \left(V_s e \frac{s}{K_s + s}\right)(c_p - Ys), \tag{18}$$

$$\frac{de}{dt} = V_e \frac{1 + K_1\bar{x} + K_2\bar{x}^2}{K_3 + K_1\bar{x} + K_2\bar{x}^2} - \left(YV_s e \frac{s}{K_s + s} + k_d\right)e, \tag{19}$$

$$\frac{dc_p}{dt} = D(Ys_f - c_p), \tag{20}$$

where $\bar{x}$ and $\bar{p}$ are given by Eqs. (9) and (10), respectively. Since the culture is in a steady state before the dilution rate is shifted, $c_p = Ys_f$ at $t = 0$. It follows from Eq. (20) that $c_p(t) = Ys_f$ for all $t > 0$. Letting $c_p = Ys_f$ in Eq. (18), we arrive at the two-dimensional system

$$\frac{ds}{dt} = \left(D - YV_s e \frac{s}{K_s + s}\right)(s_f - s), \tag{21}$$

$$\frac{de}{dt} = V_e \frac{1 + K_1\bar{x} + K_2\bar{x}^2}{K_3 + K_1\bar{x} + K_2\bar{x}^2} - \left(YV_s e \frac{s}{K_s + s} + k_d\right)e, \tag{22}$$

$$t = 0: \quad s = \tilde{s}(D_0), \quad e = \tilde{e}(D_0), \tag{23}$$

where $\tilde{s}(D_0), \tilde{e}(D_0)$ denote the steady-state substrate concentrations at the initial dilution rate D_0.

Imagine a series of experiments in which the culture is shifted from various initial dilution rates, D_0, to a fixed final dilution rate, D. Fig. 4 shows the dynamics obtained when the culture is shifted from two different initial dilution rates, $D_0 = 0.03$ 1/h and $D_0 = 0.3$ 1/h, to the final dilution rate, $D = 0.6$ 1/h.

- The dotted line is the locus of all initial (persistence) steady states. It is given by the parametric curve

  $$[\tilde{s}(D_0), \tilde{e}(D_0)], \quad 0 < D_0 < D_w,$$

  where $\tilde{s}$ and $\tilde{e}$ are given by Eqs. (14) and (15), respectively, and D_w denotes the unique washout dilution rate. As D_0 increases from 0 to D_w, the curve is traversed from the left to the right.
- The full circles denote the persistence steady state at the final dilution rate, D, and the washout steady state.
- The dashed curve is the locus of points at which the specific growth rate, r_g, equals the final dilution rate

  $$r_g \equiv YV_s e \frac{s}{K_s + s} = D.$$

  Above this dashed curve, $r_g > D$; below the curve, $r_g < D$.
- The full lines represent orbits originating from initial dilution rates $D_0 = 0.03, 0.3$ 1/h.

Note that the initial motion of the orbit is parallel to the s-axis. This represents the rapid initial increase of the substrate concentration and the specific growth rate.

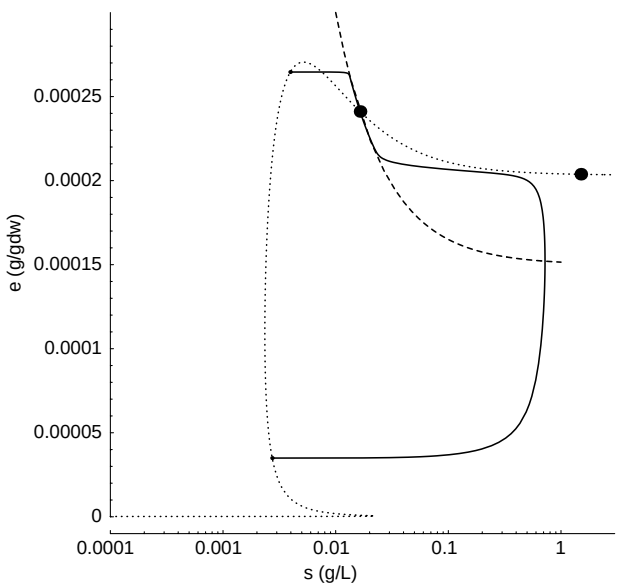

Fig. 4. Orbits for dilution rate shifts to the final dilution rate $D = 0.6$ 1/h from initial dilution rates $D_0 = 0.03$ 1/h (lower full line) and $D_0 = 0.3$ 1/h (upper full line); the feed concentration, s_f, is held fixed at 1.5 g/l.

The subsequent motion varies depending on the initial dilution rate, D_0.

If D_0 is comparable to D (see orbit for $D_0 = 0.3$ 1/h), the orbit reaches the dashed line at the end of the rapid initial motion, and then glides on it toward the persistence steady state. That is, the specific growth rate becomes equal to D almost instantaneously, and remains so subsequently. In terms of the model, this motion has the following interpretation. If D_0 is large, the initial enzyme level is so high that synthesis of new enzyme is not required in order to make the specific growth rate equal to the new dilution rate; equality is ensured by nothing more than the rapid increase of the substrate concentration. The specific growth rate remains equal to the dilution rate throughout the subsequent slow motion of the enzyme level to its final steady state value. The slow motion on the dashed line can be described by the quasi-steady state approximation

$$\frac{de}{dt} = V_e \frac{1 + K_1\bar{x} + K_2\bar{x}^2}{K_3 + K_1\bar{x} + K_2\bar{x}^2} - \left(YV_s e \frac{\bar{s}}{K_s + \bar{s}} + k_d\right)e,$$

$$0 = D - YV_s e \frac{\bar{s}}{K_s + \bar{s}},$$

$$t = 0: \quad e = \tilde{e}(D_0),$$

where $\bar{s}$ denotes the quasi-steady-state substrate concentration. This can be solved to yield

$$e(t) = \tilde{e}(D) + [\tilde{e}(D_0) - \tilde{e}(D)]\exp[-(D + k_d)t].$$

In short, the rapid initial increase of the substrate concentration is followed by a slow process during which the transport enzyme approaches its steady state exponentially fast.

If D_0 is small compared to D (see orbit for $D_0 = 0.03$ 1/h), the initial enzyme level is so small that the specific growth rate cannot match the new dilution rate even after the substrate concentration has reached supersaturating levels ($s \gg K_s$). In Fig. 4, the orbit lies below the dashed line despite the rapid increase of the substrate concentration. To mitigate this growth rate deficit, the cells begin the slow process of enzyme synthesis under supersaturating substrate concentrations. During this period, which lasts several hours (see Fig. 5), s increases and c decreases. This continues until the specific growth rate becomes equal to D. In Fig. 4, this instant corresponds to the point at which the orbit intersects the dashed curve; at this instant, s is maximal and c is minimal. The orbit then enters the region in which the specific growth rate exceeds D, and begins its final approach to the steady state. During this period, e continues to grow, but s decreases until the steady state is achieved.

The dynamics depend on the *relative* magnitude of D_0 and D. Shifting the dilution rate from $D_0 = 0.03$ 1/h to $D = 0.6$ 1/h results in large and prolonged substrate

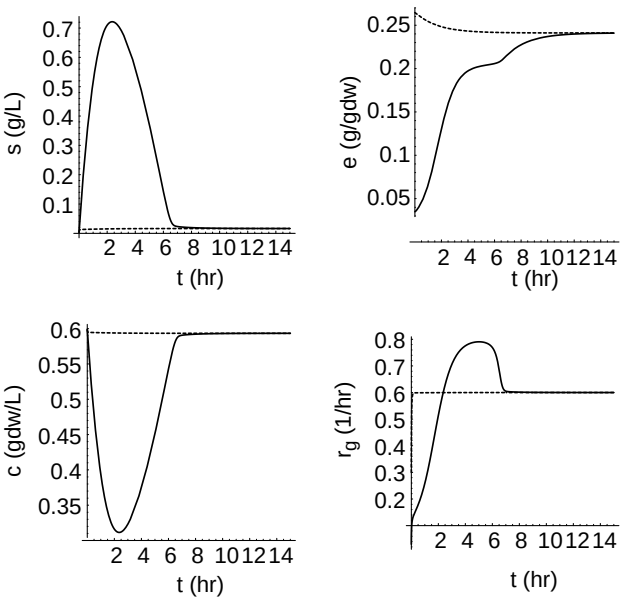

Fig. 5. Trajectories for dilution rate shifts to the final dilution rate, $D = 0.6$ 1/h, from initial dilution rates, $D_0 = 0.03$ 1/h (full lines) and $D_0 = 0.3$ 1/h (dashed lines); the feed concentration, s_f, is held fixed at 1.5 g/l.

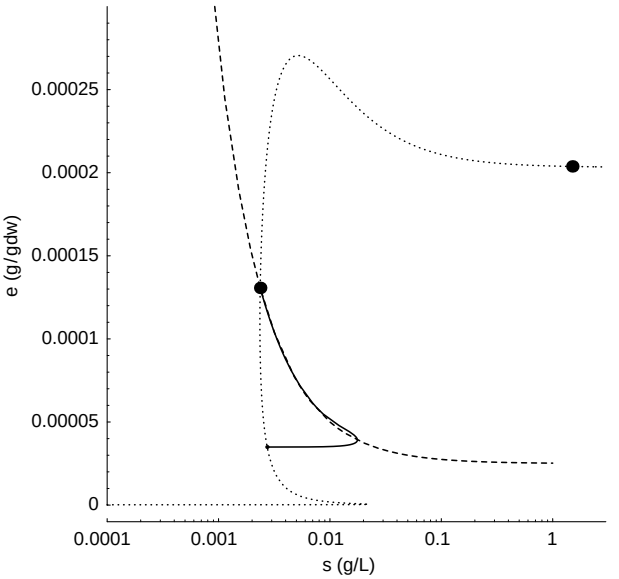

Fig. 6. Orbit for dilution rate shift to the final dilution rate $D = 0.1$ 1/h from initial dilution rate $D_0 = 0.03$ 1/h; the feed concentration, s_f, is held fixed at 1.5 g/l.

excursions (Figs. 4 and 5). But if the dilution rate is shifted from $D_0 = 0.03$ 1/h, to a lower dilution rate, $D = 0.1$ 1/h, the specific growth rate instantly equals the dilution rate, and the overshoot of the substrate concentration is imperceptibly small (Fig. 6). This is because the rapid increase of the specific growth rate resulting from an increase of the substrate concentration cannot match the dilution rate when $D = 0.6$ 1/h, but it is sufficient when $D = 0.1$ 1/h.

3.2.2. Feed concentration shifts

In these experiments, at $t < 0$, the culture is in a steady state at some dilution rate, D, and feed concentration, $s_{f,0}$. At $t = 0$, the feed concentration is abruptly increased to some value, $s_f > s_{f,0}$, while the dilution rate is held fixed. The key features of the transient response are as follows (Harrison and Topiwala, 1974)

1. The substrate concentration passes through a maximum before returning to its pre-stimulus value; the cell density, on the other hand, increases monotonically to its new steady state value (Chi and Howell, 1976).
2. The cells accommodate immediately to small changes in substrate concentration, but a lag period is characteristic of a large increase.
3. If the change in substrate concentration is large, the nature of the response depends on the dilution rate at which the feed concentration is increased (Harvey, 1970). For cells growing at high dilution rates, there is no change in the specific growth for some hours after the feed concentration is increased. For cells growing at low dilution rates, the specific growth rate accelerates immediately.

Now consider the dynamics of the model. Since the feed concentration has been increased, the initial value of the potential cell density is less than its final value; that is

$$c_p(0) = Ys_{f,0} < Ys_f = \tilde{c}_p.$$

It follows that the relation, $c_p(t) = Ys_f$, which was valid for dilution rate shifts, is no longer tenable, and the full system consisting of Eqs. (6)–(8) must be considered.

Fig. 7 shows the dynamics obtained when the system is shifted from two initial feed concentrations, $s_{f,0} = 0.1, 1.0$ g/l, to the final feed concentration, $s_f = 1.5$ g/l. In this figure

1. The line perpendicular to the s, e-plane represents the locus of all possible initial steady states. It is defined parametrically by

   $$[\tilde{s}(D), \tilde{e}(D), \tilde{c}(D, s_{f,0})], \quad 0 < s_{f,0} < s_f.$$

   The line is perpendicular to the s, e-plane because $\tilde{s}$ and $\tilde{e}$ are independent of the feed concentration. As $s_{f,0}$ increases, it is traversed upwards from the plane $\tilde{c} = 0$ to the plane $\tilde{c} = Ys_f$.
2. The full circles denote the washout and persistence steady states.
3. The full lines are the orbits corresponding to shifts from initial feed concentrations, $s_{f,0} = 0.1, 1.0$ g/l, to the final feed concentration, $s_f = 1.5$ g/l.

The evolution of the orbits in Fig. 7 is consistent with the experiments. In response to a small shift-up in the feed concentration ($s_{f,0} = 1.0$ g/l, $s_f = 1.5$ g/l), the

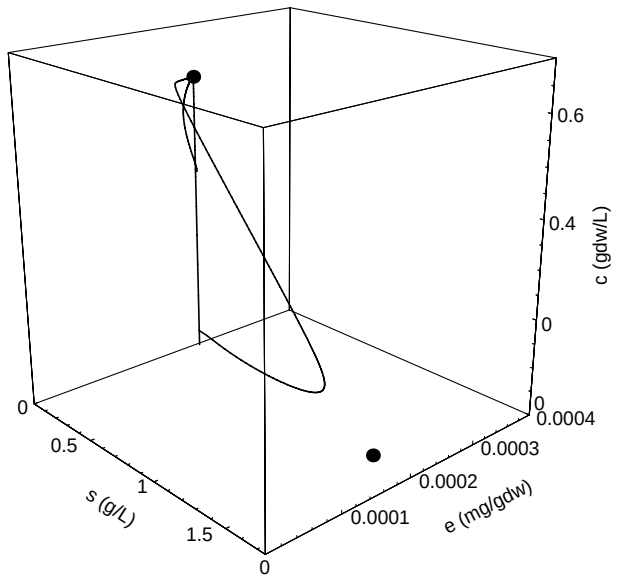

Fig. 7. Orbits for substrate concentration shifts to the substrate concentration $s_f = 1.5$ g/l from initial substrate concentrations $s_{f,0} = 0.1$ g/l (lower full line) and $s_{f,0} = 1.0$ g/l (upper full line); D is held fixed at 0.6 1/h.

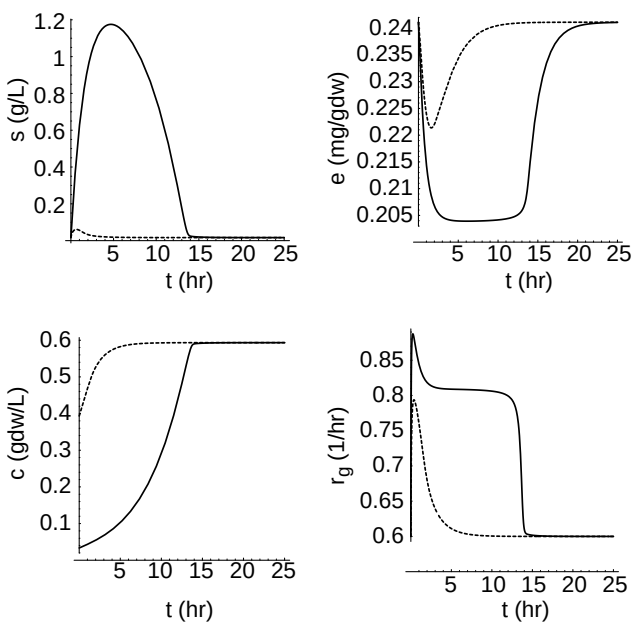

Fig. 8. Trajectories for feed concentrations to the final feed concentration, $s_f = 1.5$ g/l, from initial feed concentrations, $s_{f,0} = 0.1$ g/l (full lines) and $s_{f,0} = 1.0$ g/l (dashed lines); the dilution rate is held fixed at 0.6 1/h.

change in the substrate concentration is imperceptibly small. This is also evident in Fig. 8, which shows the solutions as functions of time. In contrast, the large substrate concentration shift from $s_{f,0} = 0.1$ g/l to $s_f = 1.5$ g/l induces a pronounced and prolonged overshoot of the substrate concentration lasting several hours. At such large substrate concentrations, $s/(K_s + s) \simeq 1$, so that the enzyme evolves without "seeing" the changes in the substrate concentration. This motion satisfies

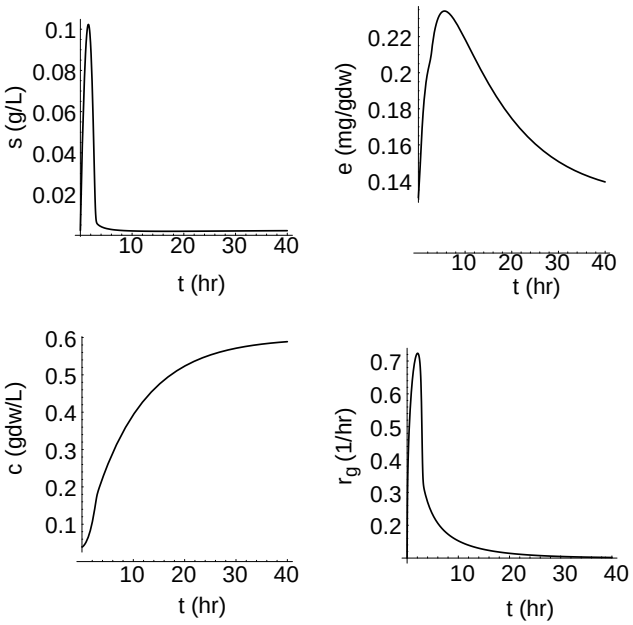

Fig. 9. Trajectories for feed concentration shifts to the final feed concentration, $s_f = 1.5$ g/l, from initial feed concentration, $s_{f,0} = 0.1$ g/l; the dilution rate is held fixed at 0.1 1/h.

the equation

$$\frac{de}{dt} = V_e \frac{1 + \bar{K}_1 e + \bar{K}_2 e^2}{K_3 + \bar{K}_1 e + \bar{K}_2 e^2} - (YV_s e + k_d)e,$$

where $\bar{K}_i \equiv K_i (V_s/k_x)^i$. In the face of this quasi-constant environment, the enzyme reaches a quasi-steady-state level, say $\bar{e}$, and the cells grow exponentially in accordance with the equation

$$\frac{dc}{dt} = (YV_s\bar{e} - D)c.$$

Now, the quasi-steady-state enzyme level, $\bar{e}$, is identical to the enzyme level that would be achieved in a batch culture of cells growing exponentially in the presence of excess substrate. But the maximum specific growth rate of a batch culture growing under substrate-excess conditions, $YV_s\bar{e}$, is very nearly equal to the washout dilution rate, D_w, of a culture growing at high substrate feed concentration (Narang, 1998). The specific rate of increase of the cell density, $d(\ln c)/dt$, therefore, equals $(D_w - D)$. The exponential growth phase persists until s becomes comparable to K_s. Finally, there begins a slow approach to the final steady state.

In the preceding simulations, the feed concentration was shifted up while the culture was maintained at a high dilution rate ($D = 0.6$ 1/h). The next simulation (Fig. 9) shows the transients in response to a large increase in the feed concentration ($s_{f,0} = 0.1$ g/l, $s_f = 1.5$ g/l) while the culture is maintained at a low dilution rate ($D = 0.1$ 1/h). It is evident that the substrate concentration overshoot is smaller and the recovery is faster (Fig. 9). This is partly because a feed concentration

shift-up at a lower dilution rate imposes a smaller burden on the chemostat—the lower the dilution rate at which the feed concentration is increased, the smaller the increment in the influx of substrate into the chemostat. But, more importantly, at high dilution rates, the substrate and inducer are initially at, or close to, supersaturating concentrations. Hence, there is little improvement in the specific substrate uptake rate, $V_s es/(K_s + s)$, despite the rapid rise in the substrate and inducer concentrations. On the other hand, at low dilution rates, both the substrate and the inducer are initially at subsaturating concentrations; the specific substrate uptake rate and the specific enzyme synthesis rate increase instantaneously in response to a feed concentration shift-up.

3.2.3. *Feed switches*

In these experiments, at time $t<0$, the culture is allowed to reach a steady state. At time $t = 0$, the identity of the growth-limiting substrate is changed while holding the dilution rate and the feed concentration fixed at their original values. Under such perturbations, it is observed that (Standing et al., 1972; Bally and Egli, 1996; Lendenmann and Egli, 1995).

1. The substrate concentration immediately increases, and the cell density rapidly decreases.
2. The magnitude of the response depends on the nature of the substrate and the dilution rate at which the identity of the substrate is switched.
   (a) If the new substrate supports a relatively large constitutive enzyme synthesis rate, the culture recovers rapidly and there is no observable substrate overshoot; if the new substrate supports a relatively small constitutive enzyme synthesis rate, there is a very pronounced lag before the excursion of the substrate concentration can be contained.
   (b) The larger the dilution rate, the longer the length of the lag.

Now consider the dynamics of the model. In general, the yields on various substrates are quite different, so that $c_p(t) \neq Ys_f$ for all t. It follows that the full system consisting of Eqs. (6)–(8) must be considered along with the initial conditions

$$s(0) = 0, \quad e(0) = e_0 = \frac{V_e}{K_3}\frac{1}{D + k_d}, \quad c(0) = c_0.$$

Here, e_0 is the steady-state enzyme level in cells growing at a dilution rate, D, in the absence of the substrate, and c_0 is the cell density of the culture on the previous substrate. The larger the value of K_3, the smaller the initial enzyme level, since the tightness of repressor-operator binding retards constitutive enzyme synthesis.

Simulations show that the time required for the chemostat to achieve the new steady state depends very strongly on K_3. When $K_3 = 10^5$, it takes 1000 h for the substrate concentration to reach values comparable to K_s. Such long lags have, and will, never be observed; therefore, we assumed that $K_3 \sim 10^4$. When $K_3 = 10^4$, the recovery time is on the order of 10 h (Fig. 10); when $K_3 = 5 \times 10^4$, the recovery time increases by an order of magnitude (Fig. 11). Both figures also show that the recovery time depends on the dilution rate at which the identity of the substrate is switched. In terms of our

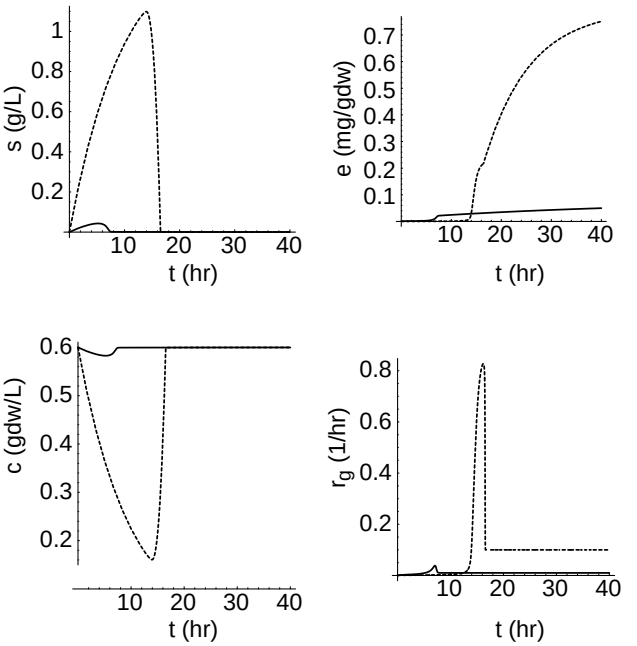

Fig. 10. Trajectories for a switch in the identity of the substrate at $D = 0.01$ 1/h (full lines) and $D = 0.1$ 1/h (dashed lines); K_3 was assumed to be 10^4.

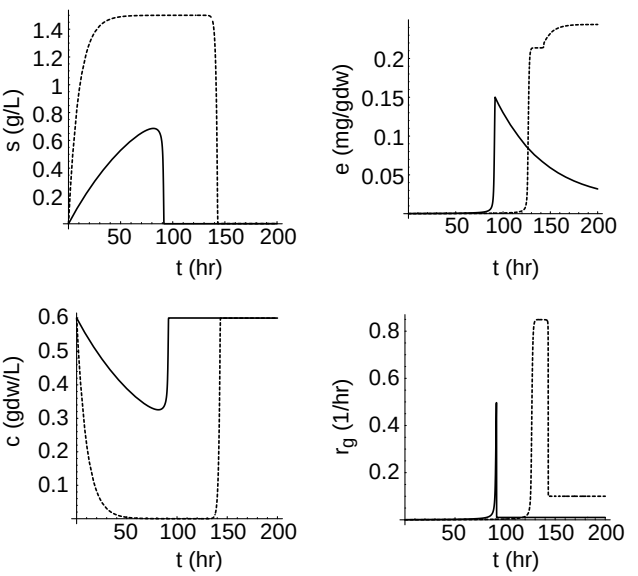

Fig. 11. Trajectories for a switch in the identity of the substrate at $D = 0.01$ 1/h (full lines) and $D = 0.1$ 1/h (dashed lines); K_3 was assumed to be 5×10^4.

model, this phenomenon has a simple explanation. At large dilution rates, the mass flow rate of the new substrate is higher and the initial enzyme level is lower; that is, a higher substrate burden is imposed upon cells that are even less capable of consuming the substrate.

3.3. Low feed concentrations

Fig. 12 shows the bifurcation diagram obtained under conditions that yield three washout bifurcation points. There are two bifurcation points in addition to the three washout dilution rates. We denote these two bifurcation points by D_h^1 and D_h^2, respectively.

The five bifurcation points decompose the D-axis into six subintervals. Fig. 14 shows the phase portraits corresponding to dilution rates in each of these intervals.

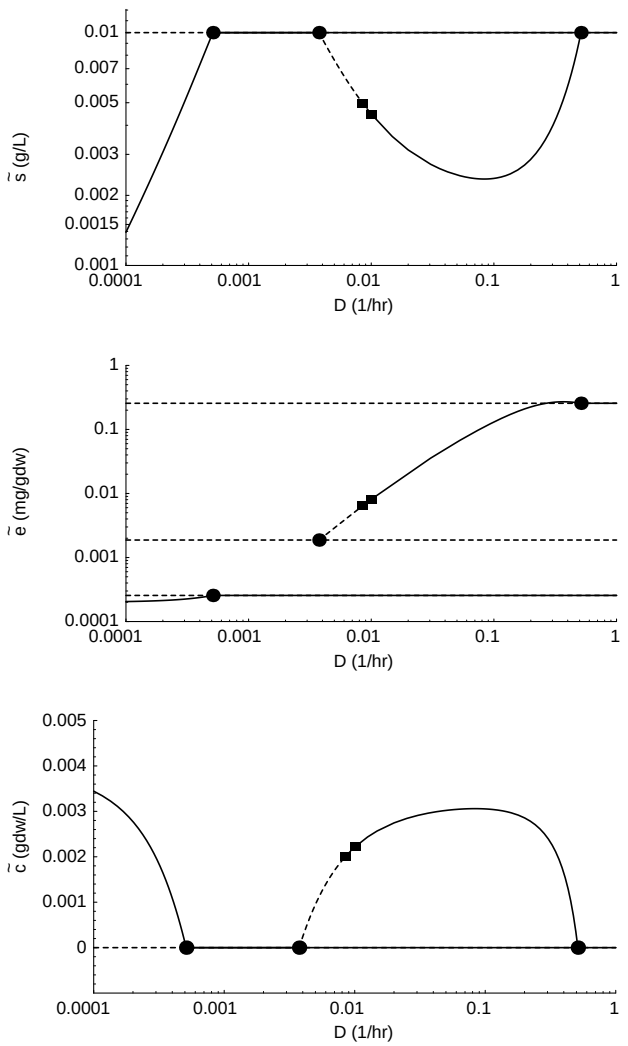

Fig. 12. Variation of steady states with D at $s_f = 0.01$ g/l. The three washout bifurcation points, $D_w^1 < D_w^2 < D_w^3$, are denoted by the symbol •; the bifurcation points at which a limit cycle is created, D_h^2, or becomes semi-stable, $D_h^1 < D_h^2$, are denoted by the symbol ▩. Stable and unstable steady states are denoted by full and dashed lines, respectively.

Note that the phase portraits contain only two variables, namely, s and e. This is because the phase portraits correspond to Eqs. (21)–(22) obtained by letting $c_p(t) = Ys_f$, a simplification that is valid only if $c_p(0) = Ys_f$. However, because c_p approaches Ys_f exponentially fast, the theory of asymptotically autonomous systems assures us that even if $c_p(0) \neq Ys_f$, the phase portraits are qualitatively similar to the phase portraits obtained by letting $c_p = Ys_f$ (Thieme, 1992). It can be seen that

1. If $0 < D < D_w^1$, all three washout steady states, ϕ_0^1, ϕ_0^2 and ϕ_0^3, are unstable, and the persistence steady state, ϕ_1, is globally stable.
2. If $D_w^1 < D < D_w^2$, then ϕ_1 ceases to exist, and the washout steady state, ϕ_0^1 becomes globally stable.
3. If $D_w^2 < D < D_h^1$, then ϕ_1 exists, but it is an unstable focus. All orbits continue to approach the globally stable washout steady state, ϕ_0^1.
4. If $D_h^1 < D < D_h^2$, then ϕ_1 is an unstable focus, but orbits emanating from it approach a stable limit cycle. Indeed, most orbits approach the limit cycle; the washout steady state, ϕ_0^1, although locally stable, has a relatively small basin of attraction consisting of initial conditions with very low enzyme levels.
5. If $D_h^2 < D < D_w^3$, then both ϕ_1 and ϕ_0^1 are stable, each with its own basin of attraction. Here, ϕ_1^0 is a stable node over the entire range, whereas ϕ_1 is a stable node only at large D. At small D, ϕ_1 is a stable focus; a shift-up to such dilution rates results in an oscillatory approach to the persistent steady state (Fig. 13) (see also Fig. 14).
6. If $D > D_w^3$, both washout steady states, ϕ_0^1 and ϕ_0^3 are stable nodes, each with its own basin of attraction.

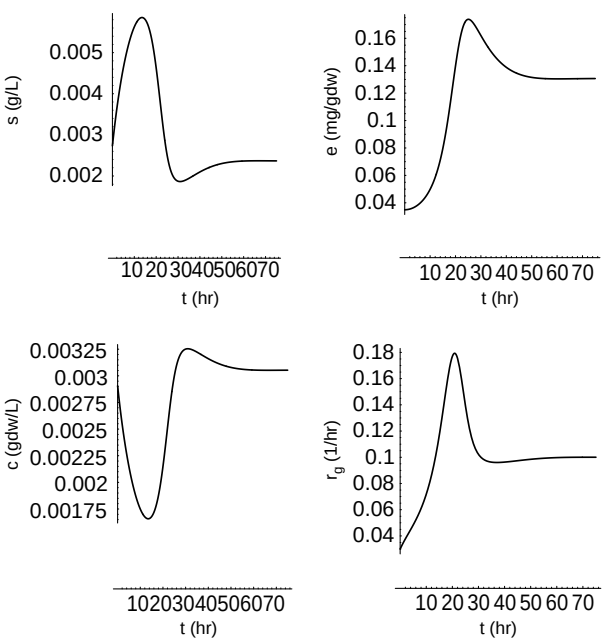

Fig. 13. Damped, oscillatory response to a dilution rate shift-up from $D = 0.03$ 1/h to $D = 0.1$ 1/h at a feed concentration of $s_f = 0.01$ g/l.

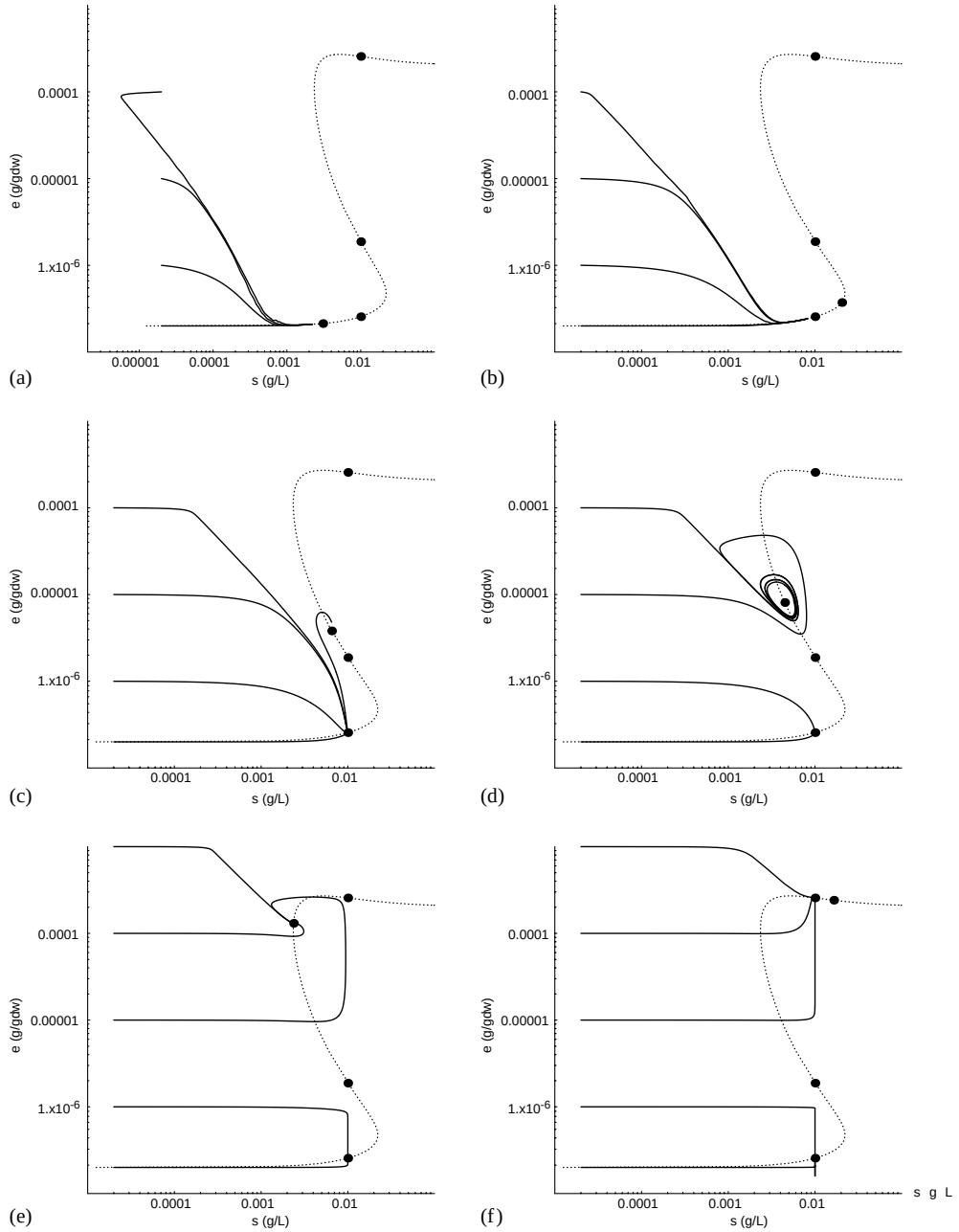

Fig. 14. Phase portraits for $s_f = 0.01$ g/l. (a) $0 < D < D_w^1$ (b) $D_w^1 < D < D_w^2$ (c) $D_w^2 < D < D_h^1$ (d) $D_h^1 < D < D_h^2$ (e) $D_h^2 < D < D_w^3$ (f) $D > D_w^3$.

Appendix C contains the stability analyses that form the basis of this classification. Here, we wish to explain the physics underlying these dynamics. In Section 3.1, we argued that sigmoidal enzyme synthesis kinetics led to washout at low dilution rates. We show below that washout at low dilution rates, in turn, implies the onset of damped and sustained oscillations. To see this, consider a chemostat operating at a persistence steady state. The stability of this steady state is determined by interactions between the following five processes: Enzyme synthesis, enzyme dilution, enzyme degradation, substrate efflux, and substrate consumption. One of these processes, namely, enzyme synthesis, is destabilizing; if the enzyme level increases, so does the rate of enzyme synthesis, resulting in even higher enzyme levels. The remaining four processes are stabilizing; if the enzyme level or substrate concentration increase, so do the rates of enzyme dilution, enzyme degradation, substrate consumption, and substrate efflux, thus restoring the chemostat to the original steady state. Now, suppose the chemostat is perturbed from away persistence steady state so that the intracellular enzyme level increases slightly. If this perturbation is imposed on a chemostat operating at a large dilution rate, the rates

of both enzyme dilution and substrate consumption increase rapidly, and restore the chemostat to the original steady state. If the same perturbation is imposed on a chemostat operating at a low dilution rate, the enzyme dilution rate is negligibly small, so that the burden of restoring the chemostat to the original steady state rests solely on the process of substrate consumption. However, when the chemostat is operated near a low washout dilution rate, the cell density is small, and this erodes the stabilizing effect of what is now the last line of defence, namely, substrate consumption. The stabilizing effect of substrate consumption now occurs with a significant time lag; the smaller the prevailing cell density, the longer the lag. At moderately small cell densities, the chemostat returns to the persistence steady state, but the motion is oscillatory, thus resulting in damped oscillations. At still smaller cell densities, the corrective effect of substrate consumption is somewhat late in coming, resulting in sustained oscillations; at the smallest cell densities, substrate consumption is so slow that the culture washes out before substrate consumption can exert its stabilizing effect. This explains the onset of damped oscillations, sustained oscillations, and washout at progressively smaller dilution rates. It is interesting, however, that the persistence steady-state regains stability at very low dilution rates. Under these conditions, enzyme synthesis, being essentially constitutive, occurs at a constant rate, and loses its ability to destabilize the chemostat.

We can make the foregoing intuitive argument more precise by considering the equation that describes the dynamics of the substrate concentration in the neighborhood of the persistence steady state. It can be shown that the deviation of the substrate concentration from its steady-state value, $\sigma \equiv s - \tilde{s}$, satisfies the equation

$$\frac{d^2\sigma}{dt^2} + (-\operatorname{tr} J)\frac{d\sigma}{dt} + (\det J)\sigma = 0, \tag{24}$$

where $\operatorname{tr} J$ and $\det J$ are the trace and determinant of the variational matrix, J, about the persistence steady state, and are given by (see Appendix C)

$$\operatorname{tr} J = \frac{\partial r_e}{\partial e} - \left(\tilde{c}\frac{\partial r_s}{\partial s} + 2D + k_d\right),$$

$$\det J = \tilde{c}\frac{\partial r_s}{\partial s}(D + k_d).$$

Eq. (24) describes the motion of a damped oscillator of unit mass, with friction coefficient, $-\operatorname{tr} J$, and spring constant, $\det J$. Now

- The stability of the steady state is completely determined by $\operatorname{tr} J$. If $\operatorname{tr} J < 0$, the friction coefficient is positive, and the substrate concentration ultimately approaches the persistence steady state; the approach is monotonic if $|\operatorname{tr} J|$ is large, and oscillatory if $|\operatorname{tr} J|$ is small. If $\operatorname{tr} J > 0$, the friction coefficient is negative, and the substrate concentration blows up.
- The terms in $\operatorname{tr} J$ are related to the response times of the various processes (Reinhart and Schuster, 1996, p. 112). Thus, $\partial r_e/\partial e$, $\tilde{c}\partial r_s/\partial s$, and k_d are the reciprocals of the response times for enzyme synthesis, substrate consumption, and enzyme degradation, respectively; the term, $2D$, is the sum of the reciprocals of the response times for enzyme dilution and substrate efflux (both processes have the response time, $1/D$).

It follows that the stability of the steady state is determined by the response times of the various processes. At high dilution rates, the rate of enzyme synthesis saturates, so that $\partial r_e/\partial e$, is small; thus, the destabilizing process of enzyme synthesis is slow, whereas the stabilizing processes of enzyme dilution and substrate efflux are fast. Under these conditions, $\operatorname{tr} J < 0$, and the steady state is stable. At low dilution rates close to washout, $\partial r_e/\partial e > 0$ is large, but D and $\tilde{c}\partial r_s/\partial s$ are small; thus, the enzyme tends to grow rapidly, but enzyme dilution, substrate efflux, and substrate consumption respond slowly. Under these conditions, $\operatorname{tr} J$ becomes positive, and the persistence steady state is unstable; any perturbation away from it leads to a limit cycle or a washout steady state.

One might argue that the occurrence of sustained and damped oscillations are an artefact of our simple model. The physics underlying these dynamics suggests that this is not the case. For, the onset of oscillatory solutions hinges crucially upon a marked attenuation of the cell density at low dilution rates. In the model, this occurs because enzyme synthesis is sigmoidal, so that enzyme levels increase faster than the dilution rate. But there is a well-established process, maintenance, which has the very same effect of reducing the cell density at low dilution rates. A more realistic model taking due account of maintenance also displays oscillatory dynamics, and it does so at all feed concentrations (manuscript in preparation).

We note finally that while the existence of three washout steady states is sufficient for the existence of a Hopf bifurcation at low dilution rates (see Appendix C for a proof of this proposition), it is by no means necessary. For the parameter values in Table 1, the Hopf bifurcation point persists at substrate concentrations as high as $s_f = 0.1$ g/l. This is because the necessary condition for the Hopf bifurcation is that $\operatorname{tr} J$ become zero. To satisfy this condition at small dilution rates, it is only necessary that the cell density be sufficiently small; it does not require that the cell density be zero.

The foregoing model predictions are consistent with the experimental data.

- In dilution rate shift-up experiments, the cell density and substrate concentrations approach their new

steady state values monotonically whenever the final dilution rate is large. However, if the final dilution rate is small, the steady state is approached via damped oscillations (Lee et al., 1976; Mor and Fiechter, 1968).

- The smaller the final dilution rate, the larger the amplitude and the period of the oscillations (Lee et al., 1976). In terms of our model, this occurs because the smaller the final dilution rate, the smaller the prevailing cell density and the larger the response time of substrate consumption. It follows that at small dilution rates, the excursions are large and prolonged before they can be contained.
- At very low dilution rates, microbial cultures are unable to grow, resulting in washout. In a number of experimental systems, this "minimum growth rate" is observed to be about 5% of the maximum specific growth rate (see Pirt, 1972 and references cited therein).

4. Conclusions

The goal of this work is to advance our understanding of dynamics of a chemostat in response to sudden changes in the flow rate, feed concentration, or identity of a single growth-limiting substrate. To this end, we have analysed a simple model accounting for induction and dilution of the transport enzyme. The parameter values of the model are based on the *lac* operon. Despite the simplicity of the model, the results are promising. We show that

- At high feed concentrations ($s_f \sim 1$ g/l), the simulations agree qualitatively with known experimental data for three types of perturbations, namely, abrupt increases in flow rate, feed concentration, and identity of the substrate. We find that in all three cases, the substrate concentration increases for several hours before it can be contained. According to our model, this occurs because the initial transport enzyme levels are too small to cope with the increased substrate supply. The magnitude of the substrate excursion is most striking when one changes the identity of the substrate feeding into the chemostat. In this case, the initial enzyme level is at its smallest since there is no prior adaptation to the new substrate; the resulting lags are on the order of several days.
- At low concentrations ($s_f \sim 0.1$ g/l), the model predicts the onset of damped and sustained oscillations at sufficiently small dilution rates. According to our model, this occurs because of the destabilizing effect of autocatalytic enzyme synthesis. At large dilution rates, enzyme dilution and substrate consumption respond rapidly, thus annihilating the destabilizing tendency of enzyme synthesis. However, at low dilution rates, both these stabilizing processes become extremely slow, leading to damped and sustained oscillations, and eventually to washout.

More data is needed to test quantitative predictions of the model. We have shown that our model yields results that agree quantitatively with the data, provided the parameter values for are suitably chosen (see Appendix B). However, to rigorously test the quantitative predictions of the model, it will be necessary to obtain transient data for a substrate such as lactose whose enzyme induction kinetics are independently measurable. Work to this effect is currently in progress in our laboratory.

Acknowledgements

We thank Prof. Lewis Johns (Chemical Engineering, University of Florida) for suggesting the analogy between the motion near a steady state and the dynamics of a linear oscillator. During the course of this research, Jason Shoemaker was supported by the University Scholars Program at the University of Florida.

Appendix A. Orders of magnitude of the parameters

The orders of magnitude of the parameters are based on kinetic properties of the *lac* operon.

1. The maximum velocity of lactose transport is 60,000 molecules per minute per permease molecule (Chung and Stephanopoulos, 1996). Since the molecular weights of lactose and permease are 342 and 46,504 (Neidhardt et al., 1987a, p. 1446), respectively
$$V_s \sim 10^4 \text{ g/gdw-h.}$$
2. The saturation constant for lactose transport is 5×10^{-4} mol/l (Chung and Stephanopoulos, 1996)
$$K_s \sim 10^{-2} \text{ g/l.}$$
3. The inducer and precursor concentrations are 10^{-3} g/gdw (Chung and Stephanopoulos, 1996) and 10^{-2} g/gdw (Neidhardt et al., 1987b), respectively. Since $D \sim 0.1$ 1/h and $Y \sim 0.1$ gdw/g, Eqs. (12)–(13) imply that
$$k_x \sim 10^3 \text{ g/gdw-h}, \quad k_g \sim 10 \text{ g/gdw-h.}$$
4. The maximum velocity of permease synthesis is 10^{-8} mol/min-l (Chung and Stephanopoulos, 1996). Since each liter of cell volume contains roughly 400 gdw
$$V_e \sim 10^{-4} \text{ g/gdw-h.}$$
5. The equilibrium constants K_1 and K_2 are 10^5 mol/l and 10^{11} (moles/l)^2, respectively (Yagil and Yagil,

1971). Since the molecular weight of the repressor ($\sim 10^5$ g/mol) is much larger than the molecular weight of the inducer ($\sim 10^2$ g/mol)

$$K_1 \sim 10^5 \text{ gdw/g}, \quad K_2 \sim 10^{11} (\text{gdw/g})^2.$$

K_3 is on the order of 10^5 (Chung and Stephanopoulos, 1996).

6. The enzyme degradation rate is on the order 0.01 1/h (Neidhardt et al., 1987a, Chapter 44)

$$k_d \sim 10^{-2} \text{ g/gdw-h}.$$

Appendix B. Comparison of model simulations with experimental data

The model provides good fits to the experimental data for a suitable choice of parameter values. We fixed the parameters, Y and K_s. The remaining parameters were determined with the software package MODFIT which selects values that minimize the square of the difference between model predictions and experimental measurements (Schittkowski, 1994). Unfortunately, experimental data on the transient response of the same microbial species to all three types of perturbations is not available. Thus, for dilution and feed concentration shift-ups, we appealed to the data obtained by Chi and Howell (1976). They measured the response of a phenol-limited culture to both dilution rate and feed concentration shift-ups. Since wall growth plays a significant role in this system, we considered the equations

$$\frac{ds}{dt} = D(s_f - s) - \left(V_s e \frac{s}{K_s + s}\right)(c + c_w),$$

$$\frac{de}{dt} = V_e \frac{1 + K_1 \bar{x} + K_2 \bar{x}^2}{K_3 + K_1 \bar{x} + K_2 \bar{x}^2} - \left(Y V_s e \frac{s}{K_s + s} + k_d\right) e,$$

$$\frac{dc}{dt} = Y V_s e \frac{s}{K_s + s}(c + c_w) - Dc,$$

$$k_x \bar{x} = V_s e \frac{s}{K_s + s},$$

$$k_g \bar{p} = Y V_s e \frac{s}{K_s + s},$$

where c_w denotes the effective volumetric cell density due to the cells attached to the wall. The optimal set of

Table 2
Parameter values used to simulate dilution rate and feed concentration shift-ups in phenol-limited cultures (Figs. 15 and 16)

$V_s = 5 \times 10^3$ g/g-h	$K_s = 6 \times 10^{-3}$ g/l	$Y = 0.5$ g/g
$k_x = 900$ g/g-h	$V_e = 5.4 \times 10^{-5}$ g/gdw-h	$K_1 = 1.2 \times 10^6$ gdw/g
$K_2 = 3 \times 10^{11}$ (gdw/g)^2	$K_3 = 7.3 \times 10^4$	$k_d = 10^{-2}$ 1/h
$c_w = 0.05$ gdw/g		

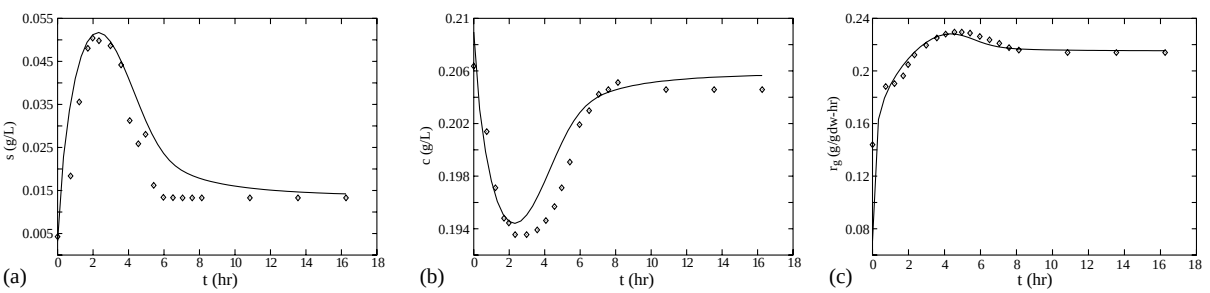

Fig. 15. Transient response of a phenol-limited culture to a dilution rate shift-up from $D = 0.11$ 1/h to $D = 0.244$ 1/h at a fixed feed concentration, $s_f = 0.7$ g/l (data from Chi and Howell, 1976). The full lines show the model simulations: (a) substrate concentration; (b) cell density; (c) specific growth rate.

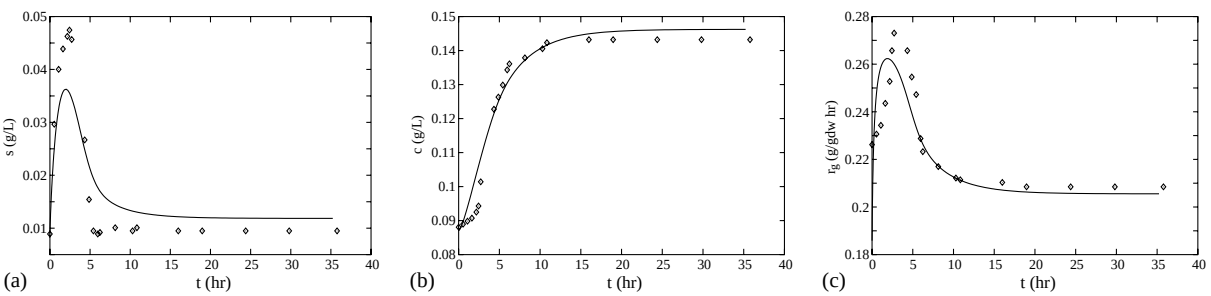

Fig. 16. Transient response of a phenol-limited culture to a feed concentration shift-up from $s_f = 0.3$ g/l to $s_f = 0.5$ g/l at a fixed dilution rate $D = 0.244$ 1/h (data from (Chi and Howell, 1976)). The full lines show the model simulations: (a) substrate concentration; (b) cell density; (c) specific growth rate.

parameters shown in Table 2 were determined in order to fit the transients observed in substrate-excess batch cultures ($r_g = 0.37$ 1/h) and a dilution rate shift-up experiment (Fig. 15). The very same set of parameters were used to simulate the feed concentration shift-up experiment (Fig. 16).

For substrate switches, we appealed to the data obtained by Bally and Egli (1996). They measured the transients obtained in *C. heintzii* cultures when the growth-limiting substrate is switched from glucose to nitrilotriacetic acid. The optimal set of parameters is shown in Table 3 and the fit to the data is shown in Fig. 17. The very same parameters also fit the data in batch cultures of nitrilotriacetic acid ($r_g = 0.17$ 1/h).

Appendix C. Global dynamics in the presence of multiple washout dilution rates

To study the asymptotic behavior of the model equations (6)–(8), it suffices to study Eqs. (21) and (22). This is because the model equations are equivalent to Eqs. (18)–(20). Now, Eqs. (20) shows that as t increases, $c_p(t)$ converges to the steady state value Ys_f exponentially fast. It follows from the theory of asymptotically autonomous systems that the asymptotic behavior of Eqs. (18)–(20) is identical to the asymptotic behavior of Eqs. (21) and (22) (Thieme, 1992). Hence, we can restrict the analysis to the dynamics generated by Eqs. (21) and (22).

Table 3
Parameter values used to simulate a substrate switch from glucose to nitrilotriacetic acid in *C. heintzii* cultures (Fig. 17)

$V_s = 2 \times 10^2$ g/g-h	$K_s = 10^{-2}$ g/l	$Y = 0.2$ g/g
$k_x = 900$ g/g-h	$V_e = 3.8 \times 10^{-4}$ g/gdw-h	$K_1 = 1.5 \times 10^5$ gdw/g
$K_2 = 2.2 \times 10^{14}$ (gdw/g)^2	$K_3 = 10^2$	$k_d = 10^{-2}$ 1/h

A.1. Washout steady states

Linear stability analysis about washout steady states shows that the eigenvalues of the variational matrix are

$$\lambda_1 = D_w^i - D,$$

$$\lambda_2 = \frac{\partial}{\partial e}[r_e(s,e) - \{Yr_s(s,e) + k_d)e\}]\Big|_{(s_f, e_w^i)},$$

where $\tilde{e}_w^i \equiv \tilde{e}(D_w^i)$ denotes the enzyme level at the washout dilution rate D_w^i. The eigenvector belonging to λ_2 is $[0,1]$ which corresponds to the invariant line $s = s_f$. It follows that

$$\lambda_2 = \frac{d}{de} g(e)\Big|_{e_w^i}, \quad g(e) \equiv r_e(s_f, e) - \{Yr_s(s_f, e) + k_d\}e.$$

Fig. 18 shows that λ_2 is negative for ϕ_0^1 and ϕ_0^3, and positive for ϕ_0^2. It follows that

- ϕ_0^1 is a saddle point for $D < D_w^1$, and a stable node for $D > D_w^1$.
- ϕ_0^2 is an unstable node for $D < D_w^2$, and a saddle point for $D > D_w^2$.
- ϕ_0^3 is a saddle point for $D < D_w^3$, and a stable node for $D > D_w^3$.

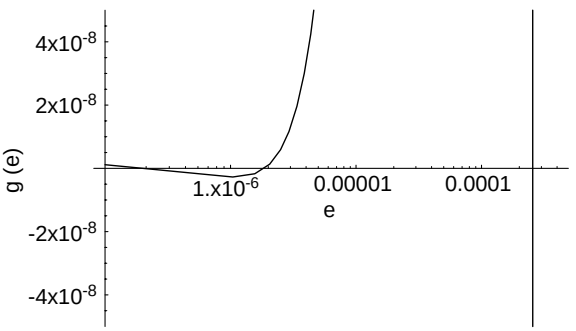

Fig. 18. Dynamics on the invariant line $s = s_f$. The plot has been truncated at $g(e) = 5 \times 10^{-8}$ in order to capture the intersection of $g(e)$ with the e-axis.

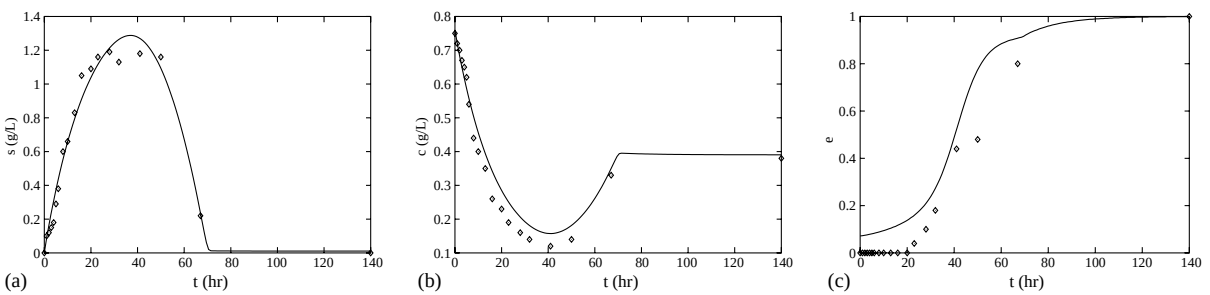

Fig. 17. Transient response of *C. heintzii* to a switch in the identity of the substrate from glucose ($s_f = 2.0$ g/l) to nitrilotriacetic acid ($s_f = 1.87$ g/l) at a fixed dilution rate $D = 0.06$ 1/h (data from (Bally and Egli, 1996)). The full lines show the model simulations: (a) substrate concentration; (b) cell density; (c) scaled enzyme level.

C.2. Persistence steady state

Linear stability analysis about the persistence steady state, ϕ_1, shows that the variational matrix, J, satisfies

$$\operatorname{tr} J = \lambda_1 + \lambda_2 = \frac{\partial r_e}{\partial e} - \left(\tilde{c}\frac{\partial r_s}{\partial s} + 2D + k_d\right), \tag{C.1}$$

$$\det J = \lambda_1\lambda_2 = \tilde{c}\frac{\partial r_s}{\partial s}(D + k_d). \tag{C.2}$$

This implies the existence of a Hopf bifurcation at some dilution rate in the interval (D_w^2, D_w^3). To see this, observe that

- As $D \to D_w^2$, ϕ_1 approaches ϕ_0^2; hence, at $D = D_w^2$, the trace for ϕ_1 equals the trace for ϕ_0^2 (which is positive). Similarly, as $D \to D_w^3$, ϕ_1 approaches ϕ_0^3, so that at $D = D_w^3$, the trace for ϕ_1 for equals the trace for ϕ_0^3 (which is negative). Since the trace for ϕ_1 varies continuously as D varies from D_w^2 to D_w^3, there must a dilution rate in the interval (D_w^2, D_w^3) at which the trace for ϕ_1 equals zero.
- The trace for ϕ_1 can be zero in two possible ways. Either the eigenvalues are real, equal in magnitude, and opposite in sign; or the eigenvalues are complex conjugates and pure imaginary (we exclude the degenerate case of two zero eigenvalues). Since $\det J > 0$, real eigenvalues cannot have opposite signs. Hence, the eigenvalues are pure imaginary, and there is a Hopf bifurcation at the corresponding dilution rate. We denote this dilution rate by D_h^2.

Stable limit cycles occur for D slightly lower than D_h^2, and damped oscillations occur for D higher than D_h^2.

References

Bally, M., Egli, T., 1996. Appl. Environ. Microbiol. 62, 133.

Baloo, S., Ramkrishna, D., 1990. Biotechnol. Bioeng. 29, 940.

Chi, C., Howell, J., 1976. Biotechnol. Bioeng. 18, 63.

Chung, J.D., Stephanopoulos, G., 1996. Chem. Eng. Sci. 51, 1509.

Domach, M.M., Leung, S.K., Cahn, R.E., Cocks, G.C., Shuler, M.L., 1984. Biotechnol. Bioeng. 26, 203.

Harrison, D.E.F., Topiwala, H.H., 1974. Adv. Biochem. Eng. 3, 167.

Harvey, R., 1970. J. Bacteriol. 104, 698.

Koch, A.L., Deppe, C.S., 1971. J. Mol. Biol. 55, 549.

Lee, I., Fredrickson, A., Tsuchiya, H., 1976. J. Gen. Microbiol. 93, 204.

Lendenmann, U., Egli, T., 1995. Microbiology 141, 71.

Maaloe, O., Kjeldgaard, N.O., 1966. Control of macromolecular synthesis: a study of DNA, RNA, and protein synthesis. Microbial and Molecular Biology, W.A. Benjamin, New York, 1966.

Mateles, R.I., Ryu, D.Y., Yasuda, T., 1965. Nature 208, 263.

Mor, J.R., Fiechter, A., 1968. Biotechnol. Bioeng. 10, 787.

Narang, A., 1998. J. theor. Biol. 190, 241.

Neidhardt, F., Ingraham, J., Schaechter, M., Brooks, K., Magasanik, B., Umbarger, H. (Eds.) 1987a. *Escherichia coli* and *Salmonella typhimurium*: Cellular and Molecular Biology, Vol. 2, American Society for Microbiology, Washington DC.

Neidhardt, F., Ingraham, J., Schaechter, M., Brooks, K., Magasanik, B., Umbarger, H. (Eds.) 1987b. *Escherichia coli* and *Salmonella typhimurium*: Cellular and Molecular Biology, Vol. 1. American Society for Microbiology, Washington DC.

Neidhardt, F.C., Ingraham, J., Schaechter, M., 1990. Physiology of the Bacterial Cell: A Molecular Approach Frank Sinauer Associates, Sunderland, MA.

Pirt, S., 1972. J. Appl. Chem. Biotechnol. 22, 55.

Powell, E., 1969. in: Malek, I., Bevan, K., Fencl, Z., Munk, V., Ricica, J., Smrckova, H. (Eds.), Continuous Cultivation of Microorganisms. Academic Press, New York, pp. 275–284.

Reinhart, H., Schuster, S., 1996. The Regulation of Cellular Systems, 1st Edition. Chapman & Hall, London.

Schittkowski, K., 1994. MODFIT: A FORTRAN code for constrained parameter estimation in differential equations and explicit model functions. Tech. Report, University of Bayreuth.

Standing, C.N., Fredrickson, A.G., Tsuchiya, H.M., 1972. Appl. Microbiol. 23, 354.

Thieme, H., 1992. J. Math. Biol. 30, 755.

Tsuchiya, H.M., Fredrickson, A.G., Aris, R., 1966. Adv. Chem. Eng. 6, 125.

Yagil, G., Yagil, E., 1971. Biochem. J. 11, 11.